THEORETICAL & APPLIED MECHANICS LETTERS **3**, 052003 (2013)

Numerical study on flow separation control over NACA0015 aerofoil using electromagnetic fields

Ahmad Sedaghat[1, a)] and Mohammad Ali Badri[2]
[1)] *Department of Mechanical Engineering, Isfahan University of Technology, Isfahan 84156-83111, Iran*
[2)] *Research Institute for Subsea Science & Technology, Isfahan University of Technology, Isfahan 84156-83111, Iran*

(Received 14 May 2013; accepted 17 July 2013; published online 10 September 2013)

Abstract In this study, a flow solver was developed based on the governing RANS equations of compressible flows and was further extended to include the effects of electromagnetic forces namely Lorentz forces. Lorentz forces may be added as a source term in the governing fluid flow equations. Numerical studies were carried out for NACA0015 aerofoil at high angles of incidences from 15° to 30° and compared with some available cases of experimental and incompressible numerical solutions. The hydrodynamics performance was improved using a magnetic momentum coefficient of up to 0.048. The size of flow separation zone was decreased or completely eliminated by increasing this coefficient. The overall drag was not changed considerably, however the overall lift was increased up to 80 percent at stall angles. © *2013 The Chinese Society of Theoretical and Applied Mechanics.* [doi:10.1063/2.1305203]

Keywords electromagnetic field, Lorentz force, flow separation, Navier–Stokes, TVD schemes

Stall occurs at high angles of incidence when large flow separation develops over control surfaces. Flow separation control using electromagnetic fields is one of the techniques which may be applied for preventing the stall occurrence. The electromagnetic field represented by the Lorentz force has been extensively used for fluids with high conductivity, such as liquid metals or semiconductor melts. For much lower electrical conductive fluids such as seawater, there is a growing application of the electromagnetic field with the aid of an additional external electrical field. Prandtl[1] showed that flow separation can be controlled using flow suction of boundary layer. Flow control techniques were consequently developed using active and passive techniques for internal and external flows. Application of electromagnetic forces to influence fluid flow or boundary layer for conducting fluids is not new and appeared as early as 1960s[2]. Some works have been conducted later on flow control of turbulent boundary layers.[3–6] In theses researches, the goal has been mainly to reduce the skin friction on wall bounded turbulent flows.

Nosenchuck et al.[3–7] have made a series of experimental investigations into the effects of reducing skin friction by employing a wall normal force arises due to electromagnetic effects, also called the Lorentz force. O'Sullivan and Bitingen[8] have made numerical studies for similar configuration as Nosenchuck et al.,[3–7] however, their results did not show such a strong reduction in skin friction. Gailitis and Lielausis[2] have used a set of regular magnetic and electric actuators on the wall to produce parallel forces with respect to surface and aimed to reduce flow separation by energizing the retarded fluid. Henoch and Stace[5] have experimentally investigated the effects of the Laurentz force on a turbulent boundary layer. Likewise, Crawford and Karniadakis[6] have numerically studied these effects. Both studies revealed a reduction in turbulent intensities whilst reported an increase in the skin friction when Lorentz force was applied. Weier et al.[9] have experimentally studied flow separation flows and its control by employing a stream wise Lorentz force parallel to the wall of the suction side of an inclined plate and a hydrofoil. Results of their study indicate that the Lorentz force enhances lift of an attached flow which is proportional to square root of the momentum coefficient. This lift enhancement was more pronounced when the Lorentz force avoids separation and cause reattached flow in the suction side of airfoil.

Akbari and Price[10] have numerically studied the dynamic stall around a NACA0012 aerofoil using a vortex method. They concluded that the reduced frequency has pronounced effect in the flow field. Robert et al.[11] have reported a comprehensive review on abrupt wing stall program in USA. Four aircraft wing configurations were studied in transonic regime and guidelines were given before flight tests. Mutschke et al.[12] have reported stall control using magneto hydrodynamic (MHD) over hydrofoils. They concluded that a more lift alleviations may be achieved if some tuned excitation frequencies were applied to the original vortex shedding frequencies. This has led to better performance on controlling lift using uniform steady Lorentz force.

Effects of a synthetic jet actuator on controlling stalled flows were also extensively reported by numerous researchers.[13–17] In all of these, the lift force was enhanced and the stall were delayed or eliminated.

For an electrically conducting fluid, the Lorentz force $\boldsymbol{f} = \boldsymbol{J} \times \boldsymbol{B}$ is defined as the vector product of the current density $\boldsymbol{J}$ and the magnetic induction $\boldsymbol{B}$. The current density is represented by Ohm's law as $\boldsymbol{J} = \sigma(\boldsymbol{E} + \boldsymbol{U} \times \boldsymbol{B})$. Here, $\boldsymbol{E}$ is the electrical poten-

[a)] Corresponding author. Email: Sedaghat@cc.iut.ac.ir.

tial, $\boldsymbol{U}$ is the flow velocity, and σ is referred as the electrical conductivity. For conducting fluids, there are two main types of flow control which are categorised as MHD problems. For high conducting fluids such as liquid metals or melting semiconductors, the flow can be adequately controlled just by employing an external magnetic field alone. As observed in $\boldsymbol{J} = \sigma(\boldsymbol{E} + \boldsymbol{U} \times \boldsymbol{B})$, the interaction of fluid velocity with the magnetic field generates an electrical current in such liquids. These magnetic generated currents will again interact with the external magnetic field to produce the Lorentz force $\boldsymbol{f} = \boldsymbol{J} \times \boldsymbol{B}$. Some low conducting electrolytes such as seawater holds a very low electrical conductivity such as $\sigma \approx 10\,\mathrm{s/m}$. Therefore, the magnetic produced electrical current (i.e., $\boldsymbol{U} \times \boldsymbol{B}$) term is so small to generate a realizable Lorentz force. To produce large current densities to alleviate a flow, some extra fields such as an external electrical field $\boldsymbol{E}$ must be applied.

The aim of the present article is to numerically investigate boundary layer separation control for hydrofoil flows. A high-resolution, time marching, implicit, and total variation diminishing (TVD) scheme is used to solve the governing fluid flow Reynolds averaged Navier–Stokes (RANS) equations. This study aims on using wall parallel Lorentz forces in the boundary layer to avoid separation in an uncontrolled separated flow over a hydrofoil usually occur at high incidence angles.

Neglecting body forces and volumetric heating, the governing fluid flows, Navier–Stokes equations in dimensionless and in the generalised transformed coordinate system is given for two dimensional flows as

$$\frac{\partial \hat{\boldsymbol{U}}}{\partial t} + \frac{\partial \hat{\boldsymbol{F}}}{\partial \xi} + \frac{\partial \hat{\boldsymbol{G}}}{\partial \eta} = \boldsymbol{S}, \tag{1}$$

$$\begin{aligned} \hat{\boldsymbol{U}} &= \boldsymbol{U}/\Gamma, \\ \hat{\boldsymbol{F}} &= (\xi_x \boldsymbol{F} + \xi_y \boldsymbol{G})/\Gamma, \\ \hat{\boldsymbol{G}} &= (\eta_x \boldsymbol{F} + \eta_y \boldsymbol{G})/\Gamma. \end{aligned} \tag{2}$$

In the above, $\xi = \xi(x, y)$ and $\eta = \eta(x, y)$ are coordinate transformation function and $\Gamma = \xi_x \eta_y - \xi_y \eta_x$ is the corresponding Jacobian which is equivalent to mesh area in finite-volume approaches. The vectors $\boldsymbol{U}$, $\boldsymbol{F}$, and $\boldsymbol{G}$ are respectively given as

$$\boldsymbol{U} = \begin{bmatrix} \rho \\ \rho u \\ \rho v \\ e \end{bmatrix}, \tag{3}$$

$$\boldsymbol{F} = \begin{bmatrix} \rho u \\ P + \rho u^2 - \tau_{xx} \\ \rho uv - \tau_{xy} \\ (e + P)u - u\tau_{xx} - v\tau_{xy} + q_x \end{bmatrix}, \tag{4}$$

$$\boldsymbol{G} = \begin{bmatrix} \rho v \\ \rho uv - \tau_{xy} \\ P + \rho v^2 - \tau_{yy} \\ (e + P)v - u\tau_{xy} - v\tau_{yy} + q_y \end{bmatrix}, \tag{5}$$

where ρ is the fluid density, (u, v) are the Cartesian velocity components, e is the total energy per unit volume and q is the heat flux. The components of shear stress tensor are as follows

$$\begin{aligned} \tau_{xx} &= \frac{\mu}{Re}\left(\frac{4}{3}\frac{\partial u}{\partial x} - \frac{2}{3}\frac{\partial v}{\partial y}\right), \\ \tau_{yy} &= \frac{\mu}{Re}\left(\frac{4}{3}\frac{\partial v}{\partial y} - \frac{2}{3}\frac{\partial u}{\partial x}\right), \\ \tau_{xy} &= \frac{\mu}{Re}\left(\frac{\partial u}{\partial y} - \frac{\partial v}{\partial x}\right). \end{aligned} \tag{6}$$

Here $Re = \dfrac{\rho_0 U_0 c}{\mu}$ is the Reynolds number based on chord c, the free stream velocity U_∞ , and the dynamic viscosity μ. The governing Navier–Stokes equations are used in non-dimensional form. The static or thermodynamic pressure is related to the total energy per unit volume as $P = (\gamma - 1)\left[e - 0.5\rho(u^2 + v^2)\right]$. Here, γ is the specific heat ratio. The source term $\boldsymbol{S}$ arises from MHD terms is given by

$$\boldsymbol{S} = \begin{bmatrix} 0 \\ J_0 B_0 \exp\left(-\dfrac{\pi}{a}\tilde{\eta}\right)\cos\theta \\ J_0 B_0 \exp\left(-\dfrac{\pi}{a}\tilde{\eta}\right)\sin\theta \\ J_0 B_0 \exp\left(-\dfrac{\pi}{a}\tilde{\eta}\right)u_t \end{bmatrix}, \tag{7}$$

where J_0 is the applied current density σE_0, B_0 is the surface magnetization of the permanent magnets, a is the span wise width of electrodes and magnets, θ is the curve angle of hydrofoil, $\tilde{\eta}$ is the vertical distance from hydrofoil, and $u_t = u\cos\theta + v\sin\theta$ is the velocity component parallel to hydrofoil surface.

Gailitis and Lielausis[2] was the first two persons who proposed to stabilize a laminar boundary layer over a flat plate using the stream wise flow control. This stream wise effect is generated by Lorentz force produced by a set of electrodes and permanent magnets with alternating polarity, as shown in Figs. 1 and 2. The generated Lorentz force direction is also shown in Fig. 2. The Lorentz force was calculated by OPERA, a software tool based on a series expansions of the magnetic and electric fields.[18] As observed in Fig. 3, the resulting force decays gradually away from the wall with an exponential distribution. A span wise variation of the force is also observed in Fig. 3 where arise from some singularities appeared in the MHD equations. Furthermore, the distribution and the amplitude of the Lorentz force can be altered by the polarity or current of the electrodes. This enables us to employ time varying forces wherever required. However, some undesirable effects such as electrochemical bubbles may occur. An average Lorentz force over the span wise coordinate z, may be given by $F = \dfrac{\pi}{8} J_0 M_0 \exp\left(-\dfrac{\pi}{a}y\right)$. Here, M_0 is the magnetization effect.

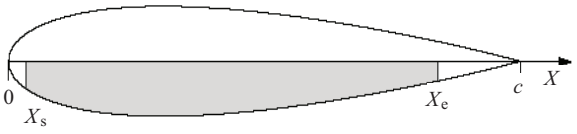

Fig. 1. Location of Lorentz force by electromagnetic operator.

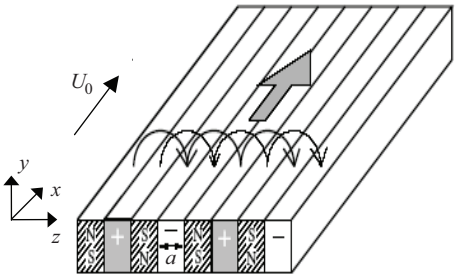

Fig. 2. Sketch of the electric (thin) and magnetic (thick) fields and resulting Lorentz force (gray arrow) over a surface.[10]

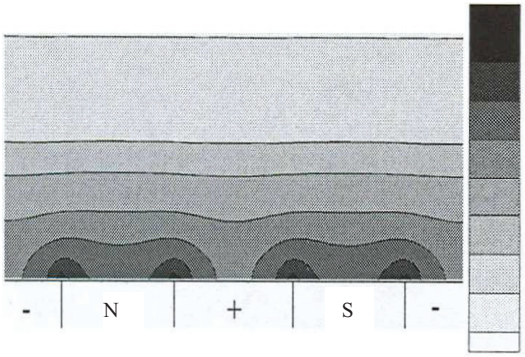

Fig. 3. Calculated Lorentz force distribution over the surface using OPERA.[18]

Tsinober and Shtem[19] have introduced a non-dimensional electromagnetic parameter $Z = \frac{\pi}{8}\frac{J_0 M_0 a^2}{\rho U_0 v}$ for MHD boundary layer with incompressible flows. This parameter represents the ratio of electromagnetic to viscous forces. It is related to the square of the Hartmann number defined for MHD flows. However, an additional non-dimensional parameter, $N = \frac{J_0 B_0 L}{\rho U_0^2}$, were also introduced.[20,21] Here, N is referred as an interaction parameter defining the ratio of electromagnetic to inertial forces, and L is a characteristic length usually taken as the chord length c of a hydrofoil. Apparently, the parameters N, Z, and Re are related by $Z/N \sim Re$. In this study $\boldsymbol{G}$ flux in the flow equations is modified with the free stream velocity of U_0 as

$$\boldsymbol{G} = \begin{bmatrix} \rho v \\ \rho uv - \tau_{xy} + \frac{J_0 B_0 a}{\pi \rho U_0^2} \exp\left(\frac{-\pi y L}{a}\right) \\ P + \rho v^2 - \tau_{yy} \\ (e+P)v - u\tau_{xy} - v\tau_{yy} + q_y + \\ u\frac{J_0 B_0 a}{\pi \rho U_0^2} \exp\left(\frac{-\pi y L}{a}\right) \end{bmatrix}. \quad (8)$$

The above discussion allows no further treatment of the numerical algorithm as far as the induced currents $\sigma(\boldsymbol{U} \times \boldsymbol{B})$ can be neglected.

The dimensionless Lorentz force in x direction with the chord length of c, is considered as

$$F^* = \frac{J_0 B_0 c}{\rho_0 U_0^2} \exp(-\frac{\pi}{a} y^* c), \quad (9)$$

The momentum magneto-hydrodynamic coefficient C_μ is also defined as[20,21]

$$C_\mu = \frac{2}{\pi}\frac{J_0 B_0 a}{\rho_0 U_0^2}\frac{x_e - x_s}{c}, \quad (10)$$

where $x_e - x_s$ is the length on which the electromagnetic operator is installed over the chord of hydrofoil (Figs. 1 and 2). x_s and x_e is set to be 0.037 48 and 0.844 07 and the overall width of operator a is set to be 0.01.

All parameters are set to their free stream values as initial condition. This means that, hydrofoil is exposed in a non-turbulent flow with free stream condition in the domain. In this case, Mach and Reynolds numbers together with angle of attack are considered as inputs. Here, dimensionless free stream velocity, molecular viscosity and density coefficients are set to unity and dimensionless pressure is determined by $p_0 = \frac{1}{\gamma M a^2}$ based on the free stream Mach number $Ma_0 = U_0/C_0$ which is the ratio of free stream velocity U_0 to the velocity of sound C_0.

No slip condition is considered as $u_{\text{wall}} = v_{\text{wall}} = 0$ and pressure gradient near the wall is ignored, i.e., $\left(\frac{\partial p}{\partial n}\right)_{\text{wall}}$. This condition for boundary layer is correct and suitable. Thermal condition is set by an adiabatic wall condition as $q_{\text{wall}} = -k'\left(\frac{\partial T}{\partial n}\right)_{\text{wall}} = 0$. where k' is condition coefficient of fluid and n is normal direction to the wall. In the prepared in-house program, a zero interpolation for pressure and temperature estimation is invoked. This means that, pressure and temperature at walls are equal to pressure and temperature near the wall. Wall temperature set as constant and equal to free stream temperature. Wall temperature in dimensionless form is given as $T = \left(1 + \frac{\gamma - 1}{2} Ma^2\right)$ and the density on the wall is determined from the pressure and temperature of the wall. For the turbulent model, parameters

on the wall are set to be zero. In the wake area and branch-cut location, a simple averaging is considered as

$$\begin{aligned}\rho_{\text{cut}} &= \frac{\rho_{\text{up}} + \rho_{\text{low}}}{2},\\ (\rho u)_{\text{cut}} &= \frac{(\rho u)_{\text{up}} + (\rho u)_{\text{low}}}{2},\\ (\rho v)_{\text{cut}} &= \frac{(\rho v)_{\text{up}} + (\rho v)_{\text{low}}}{2},\\ e_{\text{cut}} &= \frac{e_{\text{up}} + e_{\text{low}}}{2},\end{aligned} \tag{11}$$

where subscript "up" is referred to the points located up the brunch-cut and "low" to points located below it. All turbulent parameters at wake area are set equal to the trailing edge parameters.

Velocity components in Cartesian coordinate in normal and tangential are considered as $u_{\text{n}} = (\eta_x u + \eta_y v)/\sqrt{\eta_x^2 + \eta_y^2}$ and $u_{\text{t}} = (\eta_y u + \eta_x v)/\sqrt{\eta_x^2 + \eta_y^2}$, respectively. Entropy function is also defined as $s = p/\rho r$.

The developed TVD scheme with high resolution, time marching, implicit and second order accurate, is adopted here for computation of two dimensional compressible flows. The method is based on upwind and symmetric TVD schemes reported by Yee[22] and further modified by Sedaghat et al.[23,24] for computation of viscous flows. In this work, the symmetric TVD method with the MINMOD[23,24] limiter function is selected due to better predictability for low subsonic flows.

A time step based on mesh Jacobian $\Delta t_{ij} = A/(1 + \sqrt{\Gamma_{ij}})$ is considered here where A is a maximum allowable time step in whole domain and is constant. This time step is more compatible for small meshes near to surface and large meshes near the outer boundary. In this paper, $A = 0.3$ for turbulent flow is used.

To estimate the numerical convergence, the residual of ρ density is defined based on its root mean square as

$$RMS = \lg \sqrt{\frac{\sum_{i=1}^{n_\zeta} \sum_{j=1}^{n_\eta} (\rho_{ij}^{\text{new}} - \rho_{ij}^{\text{old}})^2}{n_\zeta n_\eta}}, \tag{12}$$

where n_ζ and n_η are mesh number in ζ and η direction, and ρ_{ij}^{new}, ρ_{ij}^{old} are the densities in new and old iterations at point (i, j).

In order to study grid dependency of the TVD scheme, 3 different grid sizes of 281×201, 71×51, and 141×101 are used. For the three meshes, the convergence history of the drag coefficient is shown in Fig. 4. It is observed that the result of the fine mesh of 281×201 is similar to the medium size mesh of 141×101; therefore, this later mesh is selected for the rest of computations. As also seen in Fig. 4, the number of iteration can be adopted as 2 500 iterations to achieve a converged solution.

The effects of Lorentz force are investigated in order to control flow separation over hydrofoil surfaces (as shown in Figs. 1 and 2). The location of inserting the force is presented in Fig. 1 as well. Effects of this force

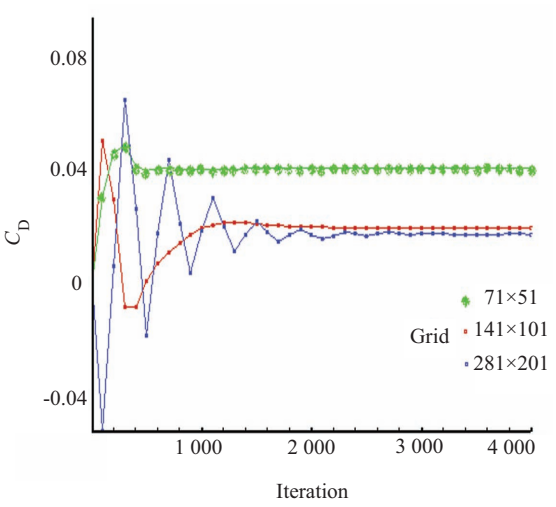

Fig. 4. Drag coefficient against number of iterations for 3 different grids.

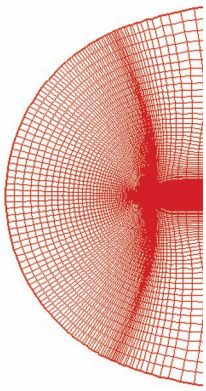

Fig. 5. Structured C-grid by 141×101.

in comparison with inertial forces is stated by magnetic momentum coefficient C_μ is further investigated. The Lorentz force is inserted into source term to model the flow pattern at Mach number 0.2 and Reynolds number 3×10^5 for NACA0015 hydrofoil. In order to investigate the flow pattern around the hydrofoil, a structured grid, type C by 141×101 grid is invoked (as shown in Fig. 5). The main advantage is omitting the separation by increasing magnetic momentum coefficient C_μ.

As it is shown in Figs. 6–8, $C_\mu = 0.048$ can completely remove separated region on upper hydrofoil surface. As observes in Fig. 6, for the state where $C_\mu = 0.0$ and the angle of attack is 18°, the separated zone begins at $x_1 = 0.23$, $y_1 = 0.08$ at the upper leading edge of the aerofoil and extend on the position $x_2 = 0.98$, $y_2 = 0.03$ where flow reattachment begins. This constitutes a zone size along 75% of the aerofoil chord length on upper surface with nearly thickness of 20% of the aerofoil chord length. This considerably reduces the aerofoil performance to the lift coefficient of the value of just $C_{\text{L}} = 1.0$.

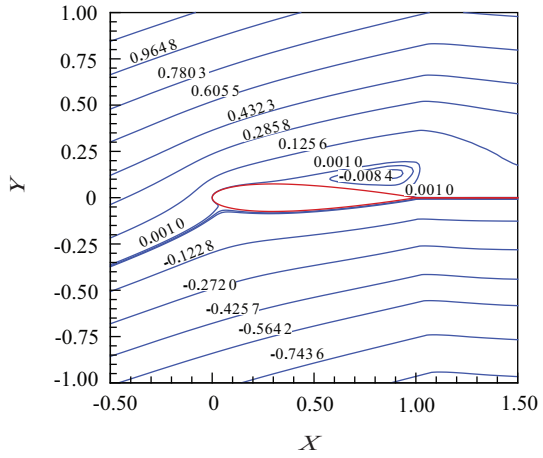

Fig. 6. Stream lines, angle of attack 18°, $C_\mu = 0$.

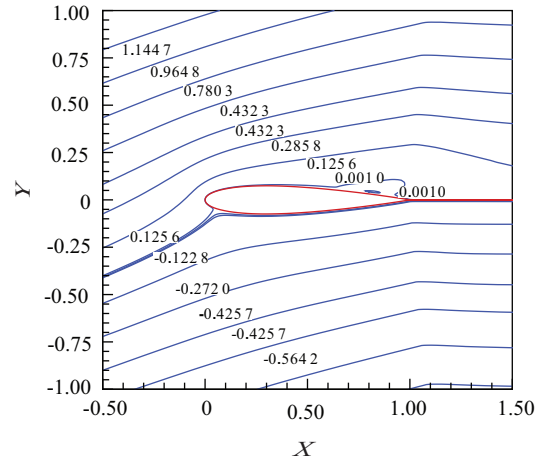

Fig. 7. Stream lines, angle of attack 18°, $C_\mu = 0.012$.

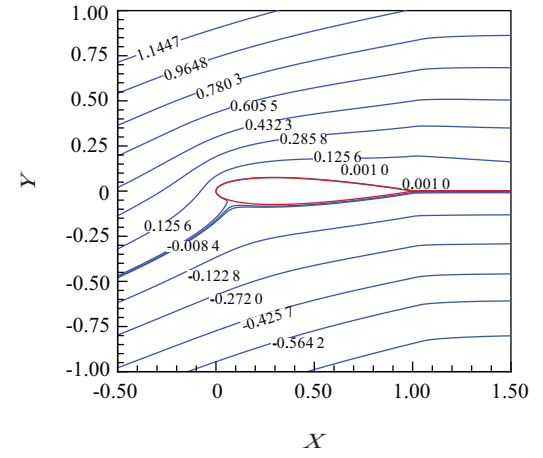

Fig. 8. Stream lines, angle of attack 18°, $C_\mu = 0.048$.

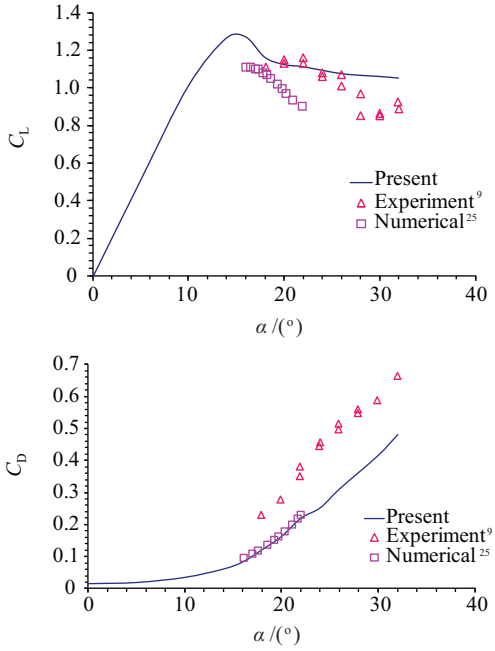

Fig. 9. Lift and drag coefficients for the NACA0015 versus angle of attack, for $C_\mu = 0, M = 0.2, Re = 3 \times 10^5$.

In Fig. 7 with $C_\mu = 0.012$ and the angle of attack 18°, the separated zone becomes smaller starts at $x_1 = 0.63$, $y_1 = 0.073$ and extend to nearly trailing edge at $x_2 = 0.94$, $y_2 = 0.03$. This makes a zone size of nearly 31% chord length of the upper aerofoil surface with approximately a thickness of 10% of the aerofoil chord length. In this case, the lift coefficient becomes $C_1 = 1.25$ which shows an enhancement of 25% lift increase in comparison with the case without separation control.

As observed in Fig. 8, the full attached flow over the upper aerofoil surface is obtained. The lift coefficient increases to the value of $C_\mathrm{L} = 1.75$ which exhibit 75% lift enhancement in comparison with the case without separation control.

Lift and drag coefficients for the NACA0015 versus angle of attack are shown in Fig. 9, up to the high value of 35°, and without magnetic control. The results are also compared with some available experimental[9] and computational[25] results based on an incompressible code. It is observed that in the stall regions where separation occurs over upper aerofoil surface, the present computation predicts lift coefficient in better agreement with experiment than an incompressible code solution. This may be related to some pressure correction methods that may be employed using incompressible codes and may suggest that compressible codes have better predictability of pressure domain than incompressible codes. As also observed in Fig. 9, the drag coefficient is under predicted the experiment in the separated region using both codes. This drawback has been reported for many turbulence models in separated regions. Lift and drag coefficients for the NACA0015 versus angle of attack is also shown

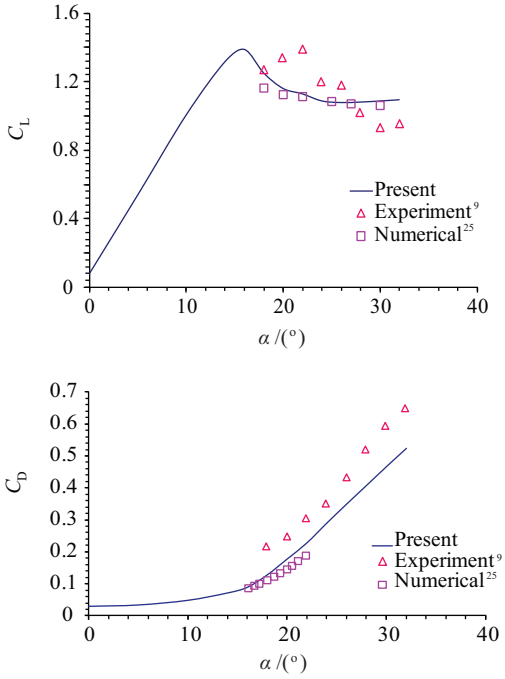

Fig. 10. Lift and drag coefficients for the NACA0015 versus angle of attack, for $C_\mu = 0.012, M = 0.2, Re = 3 \times 10^5$.

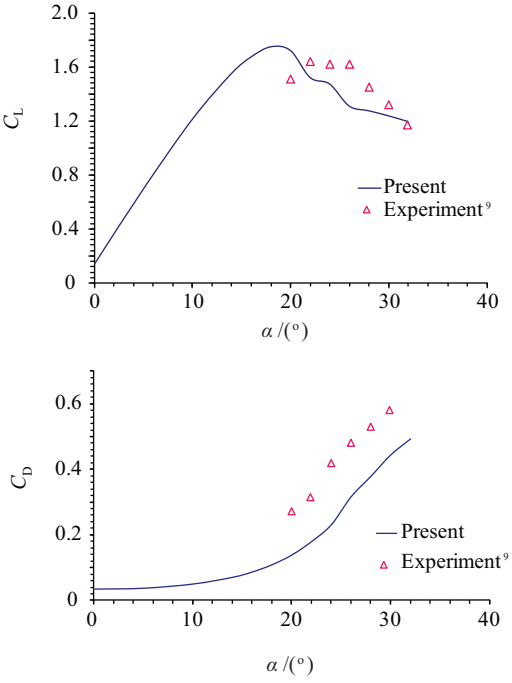

Fig. 11. Lift and drag coefficients for the NACA0015 versus angle of attack, for $C_\mu = 0.048, M = 0.2, Re = 3 \times 10^5$.

in Fig. 10 for $C_\mu = 0.012$ and in Fig. 11 for $C_\mu = 0.048$. It is seen that the lift coefficient is enhanced markedly whilst the drag coefficient is raised marginally. Both results of computations are now in better agreement with experiment by reducing size of separated region or full elimination of this region. Figure 12

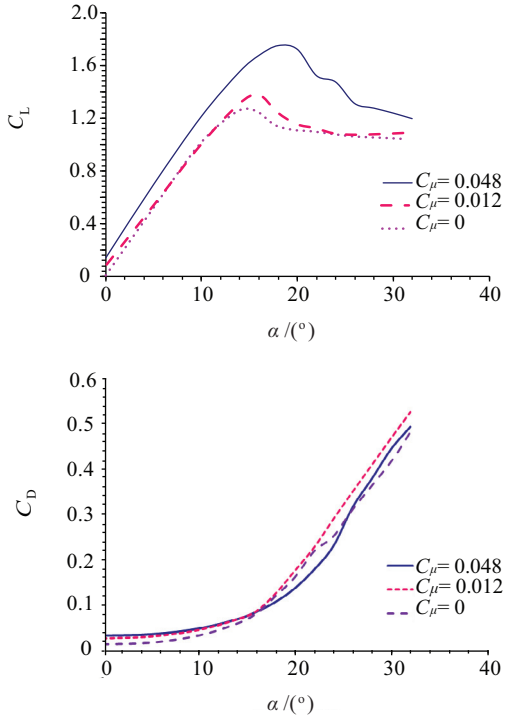

Fig. 12. Lift and drag coefficients for the NACA0015 versus angle of attack, for three different values of C_μ at $M = 0.2$ and $Re = 3 \times 10^5$.

summarises the results of lift enhancement and slight decrease of drag coefficient at three different values of the magnetic momentum coefficient C_μ. Figure 13 shows distribution of lift and drag coefficients versus momentum coefficient C_μ at high incidence angle of 18°. The results are also compared with experiments.[9] As observed, the lift enhancement trends continue by increasing C_μ whereas there is a minimum for drag coefficient at $C_\mu = 0.048$. Therefore this magnetic momentum coefficient may be optimum for the NACA0015 hydrofoil at the angle of attack of 18°. Increasing stall angle and flow stability by increasing the intensity of Lorentz force up to $C_\mu = 0.048$ are also observed here.

The effects of Lorentz force in separation prevention for a hydrofoil at high angles of attack was numerically studied. To characterize the flow separation control, the arrangement of an experimental apparatus in a water channel was adopted for comparing overall performance qualitatively. A class of high resolution TVD schemes was used for solving incompressible Navier–Stokes equations over the hydrofoil with inclusion of MHD effects. The hydrofoil was computationally set to simulate low speeds at a range of high angles of attack. In all case studies, separation was completely prohibited using the Lorentz force induced by the electromagnetic field. By increasing angles of incidence, the lift coefficient as well as the drag coefficient over the hydrofoil was increased. However, lift gain was greater than drag increase. By this investigation, it was evident that the current computational fluid dynamics (CFD) code can be used to

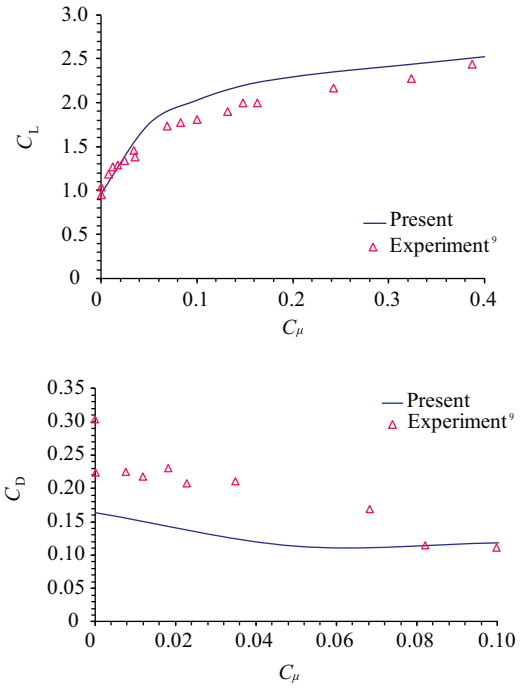

Fig. 13. Lift and drag coefficients for the NACA0015 versus different values of C_μ at $\alpha = 18^\circ, M = 0.2, Re = 3 \times 10^5$.

accurately calculate flow fields in presence of electromagnetic fields. Hence, a wide range of flow conditions can be studied using this tool. The MHD concept may be used to increase performance of hydrofoils as well as airfoils at high speeds.

In overall, the range of applicability of electromagnetic field may be evaluated computationally for preventing the stall phenomenon. With the growing number of techniques in flow control, computational results for a hydrofoil may give guidelines for developing electromagnetic systems in the new generation of underwater vehicles.

1. L. Prantdl, *Fluid flow in very little friction*. Proceedings of the Third International Maths Congress, Heidelberg (1904).
2. A. Gailitis and O. Lielausis, *Applied Magnetohydrodynamics. Reports of the Physics Institute* (AN Latv. SSR, 1961) **12**, 143.
3. D. M. Nosenchuck and G. L. Brown, *Near Wall Turbulent Flows*, edited by R. M. C. So, C. G. Speziale, and B. E. Launder (Elsevier, 1993) 689.
4. J. C. S. Meng, C. D. Henoch, and J. D. Herbes, Magnetohydrodynamics **30**, 401 (1994).
5. C. Henoch and J. Stace, Phys. Fluids **7**, 1371 (1995).
6. C. H. Crawford and G. E. Karniadakis, Phys. Fluid **9**, 788 (1997).
7. D. M. Nosenchuck, G. L. Brown, H. C. Culver, et al., *Spatial and temporal characteristics of boundary layers controlled with the Lorentz force*, Proceedings of 12th Australian Fluid Mechanics Conference, Sydney (1995).
8. P. L. O'Sullivan and S. Biringen, Phys. Fluids **10**, 1181 (1998)
9. G. Weier, G. Gerbeth, O. Mutschke, et al., SFB-Preprint SFB609-03 (2004).
10. M. H. Akbari and S. J. Price, Journal of Fluids and Structures **17**, 855 (2003).
11. M. Robert, H. Shawn, H. Woodson, et al., Progress in Aerospace Sciences **40**, 417 (2004).
12. G. Mutschke, G. Gerbeth, T. Albrecht, et al., European Journal of Mechanics-B/Fluids **25**, 137 (2006).
13. R. Duvigneau and M. Visonneau, Aerospace Science and Technology **10**, 279 (2006).
14. R. Duvigneau and M. Visonneau, Computers & Fluids **35**, 624 (2006).
15. H. Tang and S. Zhong, Aerospace Science and Technology **13**, 331 (2009).
16. A. Qayoum, V. Gupta, P. K. Panigrahi, et al., Sensors and Actuators A: Physical **1629**, 36 (2010).
17. M. Jain, B. Puranik, and A. Agrawal, Sensors and Actuators A: Physical **165**, 351 (2011).
18. E. Grieberg, *Applied Magnetohydrodynamics, Reports of the Physics Institute* (AN Lav. SSR, 1961) **12**, 147.
19. A. B. Tsinober and A. G. Shtern, Magnitnaya Gidrodinamica **3**, 152 (1967).
20. T. Weier, U. Fey, G. Gerbeth, et al., ERCOFTAC Bulletin **44**, 36 (2000).
21. T. Weier, G. Gebeth, G. Mutschke, et al., Experimental Thermal and Fluid Science **16**, 84 (1998).
22. H. C. Yee, J. Comp. Phys. **57**, 327 (1985).
23. A. Sedaghat, *A finite volume TVD approach to transonic flow computation* [Ph.D. Thesis], The University of Manchester, Manchester (1997).
24. A. Sedaghat, S. Shahpar, and I. M. Hall, *Drag reduction for supercritical aerofoils*, Proceedings of 20th ICAS Congress, Sorrento, Italy (1996).
25. N. Folladi, M. R. Jahan Nama, and F. Mohaghegh, *Separation control over hydrofoil surface using electro-magnetic*, Proceedings of 13th ISME conference, Isfahan (2005).